The 2010 IEEE/RSJ International Conference on
Intelligent Robots and Systems
October 18-22, 2010, Taipei, Taiwan

Exploiting Proximal F/T Measurements for the iCub Active Compliance

Matteo Fumagalli, Marco Randazzo, Francesco Nori, Lorenzo Natale, Giorgio Metta and Giulio Sandini

Abstract— **During the last decades, interaction (with humans and with the environment) has become an increasingly interesting topic of research within the field of robotics. At the basis of interaction, a fundamental role is played by the ability to actively regulate the interaction forces. In this paper we propose a technique for controlling the interaction forces exploiting a proximal six axes force/torque sensor. The major assumption is the knowledge of the point where external forces are applied. The proposed approach is tested and validated on the four limbs of the iCub, a humanoid robot designed for research in embodied cognition. Remarkably, the proposed approach can be used to implement active compliance in other non passively back-drivable manipulators by simply inserting one or more force/torque sensor anywhere along the kinematic chain.**

I. Introduction

Robot interaction has been hypothesized to be at the basis of cognitive processes [1]. Through interaction, cognitive systems create their own knowledge (their epistemology) of the surrounding environment. These concepts are at the basis of a new research direction that mixes robotics and research in cognitive systems, where robots and humans share the same physical space [2]. In this sense, *safety* becomes necessary in unstructured environments. In this context, autonomous behavior and learning capabilities are fundamental, and the role of perception and sensor integration becomes of primary importance [3]. Within this framework, force information covers an important role for the exploration process during the interaction of the robot with the environment and humans. Force control here can be considered as a tool of the learning phase, which contributes to preserve the robot and its surrounding environment. The ability to detect and counteract forces helps in preserving the robot own safety and that of the environment (including people). Compliance plays a central role for the interactive and explorative behavior of the robot. Robot safety has been considered in [2] and [4]. All aspects of robot design should be considered in order to increase safety [5]: mechanics design but also software, and electronics. From the mechanical point of view, passive compliance has the peculiarity of decoupling the link and rotor inertias, thus resulting in an intrinsically safe actuation system [5], [6]. Light-weight designs have also been investigated in [7] where it is shown that impact forces can be reduced, resulting in a safer robot. Similarly, the macro-mini actuation design proposed in [8] relies on relocating the major source of actuation at the base of the manipulator while employing light-weight and small motors which maintain high-frequency torque capability without increasing the overall system size.

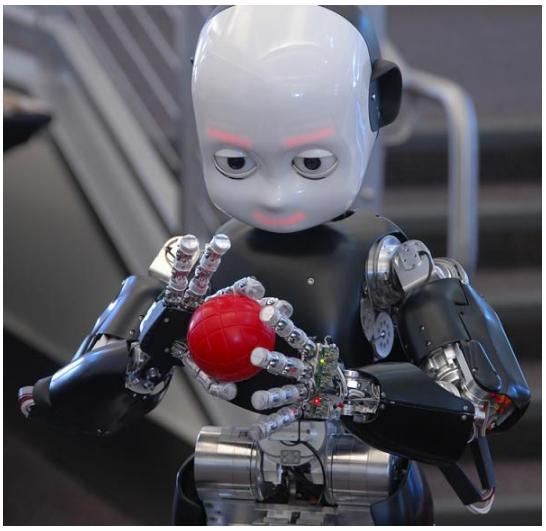

Fig. 1. The iCub humanoid robot.

An alternative to these mechanical solutions is the implementation of active force control on non back-drivable manipulators. Even though this approach is far from being intrinsically safe, it does not require to increase the complexity of the mechanical system. Standard industrial approaches employ a single 6-axis Force/Torque (F/T) sensor located in a distal configuration, e.g. at the end effector of the manipulator [9]. The obvious assumption in this case is that the robot interaction with the environment only occur distally at the tool level. Joint torque sensing might be an alternative solution to this issue [10], [11], but it again requires a specific joint design for torque sensing.

The solution proposed in this paper consists in exploiting one (or more) F/T sensor placed in a proximal configuration[1]. In our interpretation, this solution can be seen as an intermediate alternative which merges some of the benefits of localized (distal) F/T sensing together with some advantages of distributed joint torque sensing. As clearly described later in the paper, a proximal sensor allows measuring forces applied at different levels (not only at the end-effector) and gives information about joint torques.

In this paper we first present the iCub, the humanoid

M. Fumagalli, M. Randazzo, F. Nori, L. Natale, G. Metta and G. Sandini are with the Robotics, Brain and Cognitive Sciences Department, Italian Institute of Technology, Genoa, Italy. Corresponding author email: matteo.fumagalli@iit.it

G. Metta is also with the Department of Communication, Computer and System Sciences, Faculty of Engineering, University of Genoa, Italy

[1]Within this framework, proximal, as opposed to distal, refers to the natural order of joints in an open kinematic chain. Therefore, proximal refers to objects close the base of the chain. Distal refers to objects close to the end-effector.

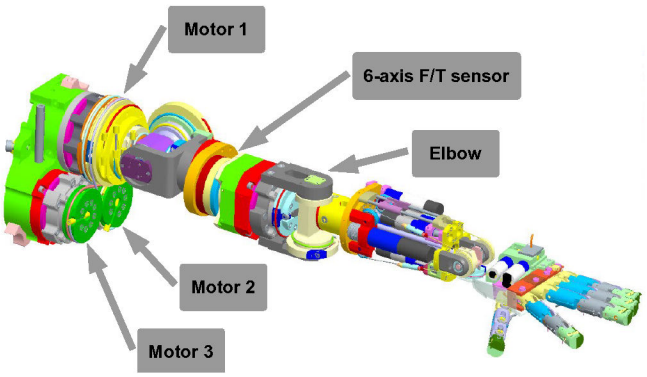

Fig. 2. The iCub arm. A CAD view of the shoulder joint mechanism showing the three motors actuating the joint and the pulley system, the F/T sensor, the elbow and the hand.

platform where our approach has been tested. Section II describes the mechanics, the electronics and the software structure. Subsection II-F describes our custom F/T sensors which have been employed for experiments. Section III presents a technique for implementing a force and an impedance controller exploiting a proximal F/T sensor. Finally, section IV presents some experimental results.

II. THE ICUB PLATFORM

The iCub humanoid robot has been designed with the goal of creating an open hardware/software robotic platform for research in embodied cognition [12]. Its design has been mainly developed within RobotCub[2] a European funded project with the goal studying natural and artificial cognitive systems [13]. As a major design specification, the iCub should be capable of interacting with humans and environments using its sensors to react in response to external events.

At the current state, the iCub robot has a total of 53 degrees of freedom (DOF), 6 in each leg, 7 in each arm, 6 in the head, 3 in the waist and 9 for each hand. The iCub employs brushless and brushed DC motors equipped with high reduction gearboxes (1:100 or bigger). This solution allows compact designs but makes the robot passively non back-drivable. As a major consequence of this design choice, the only way to implement an effective force control for the iCub consists in implementing an active force feedback controller as the one proposed in this paper.

Employed motors can be divided into two broad categories: brushless and brushed DC motors. Typically brushless motors have been employed in the bigger articulated joints (shoulders, elbows, hips, torso, knees) while small brushed motors actuate the distal degrees of freedom (hand joints, neck, eyes). Remarkably, non standard mechanical choices have been used to rise the torque/volume ratio as will be briefly shown in next subsections. Particular attention will be given to the shoulder mechanism.

[2]RobotCub project IST-FP6-004370.

A. Arm

The arm is a 7DOF manipulator. Its upper part is commanded by four brushless motors, three for the shoulder movements and one for the elbow. The shoulder joint is a cable differential mechanism with a coupled transmission system (see Fig. 2). Three coaxial motors housed in the upper-torso move pulleys to generate the spherical motion of the shoulder [10], [12].

The motor groups are brushless frameless motors (RBE Kollmorgen series) with harmonic drive reductions (CSD series with 100:1 ratio) [12]. These motors are located in the torso frame. A first bigger actuator (Motor 1 in Fig. 2) is capable of delivering $40Nm$ and two medium power motors (Motor 2 and Motor 3) provide $20Nm$ each.

The first motor actuates directly the first joint (shoulder pitch), whereas the second and third motors actuate two pulleys that are coaxial with the first motor. The motion is transmitted from the motors to the joints through idle pulleys. Joint positions are measured by Hall effect sensors with custom made electronics. The shoulder coupling T_{mj} between the motor angular velocities $[\dot{\theta}_{m1}, \dot{\theta}_{m2}, \dot{\theta}_{m3}]^\top = \dot{\theta}_m$ and joint velocities $[\dot{\theta}_{pitch}, \dot{\theta}_{roll}, \dot{\theta}_{yaw}]^\top = \dot{\theta}_j$ has the following linear form:

$$\dot{\theta}_m = T_{mj}\dot{\theta}_j \qquad T_{mj} = \begin{bmatrix} 1 & 0 & 0 \\ -r & r & 0 \\ -2r & r & r \end{bmatrix}, \qquad (1)$$

where r is a constant value which depends on the radius of the pulleys. The torques at joint level τ can be transformed into the equivalent motor torques τ_m by the following equation [14]:

$$\tau_m = T_{mj}^{-\top}\tau, \qquad (2)$$

where $A^{-\top}$ indicates the transposed inverse of a matrix A. Differently from the shoulder, the elbow joint has an independent frameless brushless motor. The joint is commanded with tendons in push-pull configuration, moving an idle pulley.

The wrist is a 3DOF manipulator. The roll movement (i.e. the movement competing for the pronosupination of the wrist) is achieved by a single brushed motor directly coupled to the forearm. The pitch and yaw movements instead are accomplished by two motors, which move a semi-differential mechanism through tendons. Brushed motors have been employed for the wrist joints. Positions are measured through magnetic incremental encoders mounted on the motors.

B. Hand

The hand is a tendon driven mechanism with 9DOF. Seven motors are placed remotely in the forearm and all tendons are routed through the wrist mechanism. Two motors are mounted directly on the hand: one of the motors controls the thumb abduction and the other actuates the fingers adduction/abduction. Both these joints are sensorized with tiny Hall effect position sensors. Similarly, finger positions are measured using 15 Hall effect sensors directly mounted on the phalanxes (three for each finger). Adopting these solutions allows a design with very limited dimensions: the

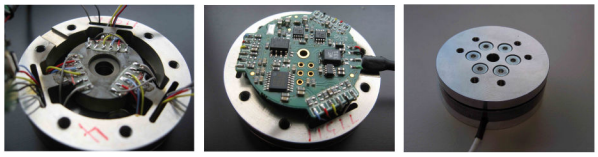

Fig. 3. The custom F/T sensor. Picture of the sensing element (top) and of the embedded board (bottom left). The assembled sensor (bottom right) exits with sampled digital signal directly over a CAN-bus line, with a rate of $1ms$.

palm is $50mm$ long, $34mm$ wide at the wrist and $60mm$ wide at the fingers. The overall thickness of the hand is only $25mm$.

C. Head and Waist

The neck structure is a 3DOF serial manipulator which allow the pitch, roll and yaw movements of the head. The eyes exploit three brushed motors to control independently the pan and to simultaneously control the tilt. The head also mounts two cameras which represent the iCub vision system,

The waist mechanism is a 3DOF kinematic chain [12], [15]. It makes use of a tendon-driven differential mechanism for pitch and yaw movements using two brushless motors. Similarly to the shoulder actuation, the motor velocities $[\dot{\theta}_{m1}, \dot{\theta}_{m2}]^\top = \dot{\theta}_m$ and the joint velocities $[\dot{\theta}_{pitch}, \dot{\theta}_{yaw}]^\top = \dot{\theta}_j$ are kinematically coupled by a linear relation:

$$\dot{\theta}_m = T_w \dot{\theta}_j \qquad T_w = \begin{bmatrix} r & r \\ -r & r \end{bmatrix}, \tag{3}$$

where r is a constant value which depend on the dimension of the pulleys. An equation equivalent to (2) holds between the joint and motor torques, τ and τ_m respectively. A third motor, placed in between the aforementioned mechanism compete for the roll motion. This configuration allows a better distribution of the joint torque on the motors, thus allowing a reduction of the mechanism dimension.

D. Legs

Legs are 6DOF serial manipulator [12], [15]. All the six motors are frameless brushless (RBE Kollmorgen series) equipped with harmonic drive reduction of $100 : 1$ (CSD series).

E. Electronics and Sensors

Motors are commanded with custom electronic boards mounting a Freescale 56F807 DSP. The control rate of these boards is $1ms$. Joint angles make use of analog Hall effect based sensors directly connected to the boards. CAN-bus lines are employed for the communication between the boards. All communication lines converge to a PC-104 board whose principal role is to collect and synchronize all the sensory and motor data. A gigabit Ethernet interface allows the PC-104 to communicate with an external network, typically used for intensive data processing.

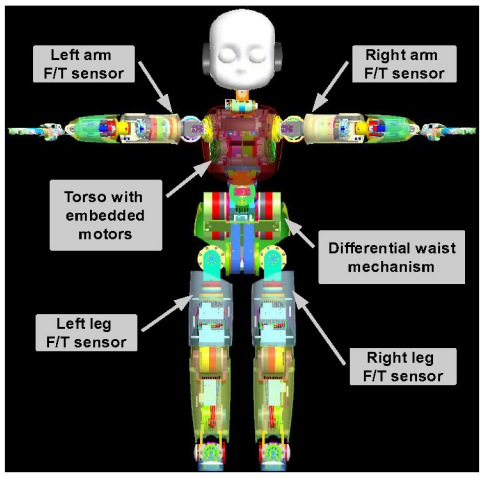

Fig. 4. A CAD view of the iCub robot. Some particular mechanism and the F/T sensors location are highlighted.

F. The force/torque sensor

All the four iCub limbs are equipped with custom made F/T sensors [15]. In the arms these sensors are placed in the upper part, in between the shoulder and the elbow; in the legs the sensor are located in between the hip and the knee (see Fig. 4). These F/T sensors employ semiconductor strain gauges for measuring the deformation of the sensing elements. The signal conditioning and the analog to digital converters are embedded in the sensor. The data processing is performed on a 16 bit DSP from Microchip (dsPIC30F4013). The associated circuitry samples and amplifies up to 6 analog channels which can be used to measure the voltage across 6 strain gauges in a Wheatstone bridge configuration. The analog to digital converter (AD7685, 16 bit, 250 Ksps, SPI interface) is multiplexed (ADG658) on the 6 channels and amplified with a standard instrumentation amplifier (INA155).

The F/T sensor position just described, differs from the classical distal configuration at the end-effector [9]. Specifically, the iCub F/T sensors are mounted proximally in each limb. This solution has different advantages:

- The F/T measurements give information about the arm internal dynamic.
- External forces applied on the arm (e.g. not only forces applied at the end-effector) can be sensed.
- Information about the actual joint torques can be extracted from the the proximal F/T sensor.

G. YARP:

The iCub software is based on Yarp [13]. Yarp is a set of open source, OS-independent libraries that support hardware and software modularity. Hardware modularity is obtained by defining interfaces for classes of devices in order to wrap native code API. In this way, a change in hardware requires only a change in the API calls. Yarp supports also software modularity, providing an inter-process communication protocol based on ports, which allows the user to subdivide the main task of the robot in simple, reusable modules,

each of them providing specific functionalities (e.g. object tracking, grasping etc). The user application is then obtained by interconnecting at run-time these software modules, which can also run on different machines on a common network, in order to obtain more complex behaviors.

III. Force Control

In this section we describe the active compliance controller, which has been implemented on the iCub; the proposed procedure exploits only the proximal F/T sensors. As described in Section II-F, the position of the sensor is such that the given measurements detects both internal (i.e. due to internal dynamics) and external forces. This concept is better formalized Section III-A. The following notation is adopted: angular brackets $\langle\cdot\rangle$ are used for Cartesian reference frames; a vector $v \in \mathbb{R}^3$ expressed in the reference frame $\langle a\rangle$ is denoted v^a; similarly a wrench $F = [f, \mu] \in \mathbb{R}^6$, i.e. the composition of a force $f \in \mathbb{R}^3$ and a torque $\mu \in \mathbb{R}^3$, will be denoted F^a when represented in $\langle a\rangle$. The roto-translation transforming vectors from $\langle a\rangle$ to $\langle b\rangle$ is represented by a rotation R_a^b and a translation p_a^b. Therefore a wrench F^a can be represented in $\langle b\rangle$ as follows [9]:

$$F^b = T_a^b F^a, \quad T_a^b = \begin{bmatrix} R_a^b & 0 \\ 0 & R_a^b \end{bmatrix}.$$

Finally, a wrench F_a applied in $\langle a\rangle$ has an equivalent wrench F_b (i.e. a wrench that generate the same work for every possible rigid body motion) applied in $\langle b\rangle$ which can be computed as follows (see [14] pag. 120):

$$F_b^b = H_a^b F_a^a, \quad H_a^b = \begin{bmatrix} R_a^b & 0 \\ S(p_a^b)R_a^b & R_a^b \end{bmatrix},$$

where $S(v) \in \mathbb{R}^{3\times 3}$ is the operator performing the cross product $v\times$.

A. Internal and external measurement

As previously pointed out, the wrench F_s measured at the sensor reference frame, hereafter denoted $\langle s\rangle$, is the sum of two terms, one due to the limb internal dynamics, the other due to an external wrench F_e. The assumption here is that F_e is the unique external perturbation and that this perturbation is applied in a known reference frame, denoted $\langle e\rangle$. Without loss of generality we assume that $\langle e\rangle$ corresponds to the reference frame attached at the end-effector. Expressing all these quantities in $\langle s\rangle$, we can conclude that our measurement $F_s^s \in \mathbb{R}^6$ can be decomposed as follows:

$$F_s^s = F_e^s + F_i^s \ , \tag{4}$$

where $F_i^s \in \mathbb{R}^6$ is the contribution of the manipulator internal dynamics to our measurement F_s^s. Moreover, it can be shown that[3]:

$$F_i^s = M_F(q)\ddot{q} + C_F(q,\dot{q})\dot{q} + g_F(q), \tag{5}$$

[3]Equation (5) can be computed by applying slight modifications to the classical Newton-Euler formulation as described in Chapter 4 Section 5 of [14]. A complete description of this procedure lays outside the scope of the paper.

where $q \in \mathbb{R}^n$ is the generalized coordinates vector describing the configuration of the limb, here assumed composed of n DOF. The internal force F_i^s depends on joint position q, velocities $\dot{q}$ and acceleration $\ddot{q}$ and it can be decomposed in the sum of an inertial term $M_F(q) \in \mathbb{R}^{6\times n}$, a gravitational term $g_F(q)$ and a Corioli's terms $C_F(q,\dot{q})\dot{q}$. It has been already shown [16] that the internal dynamic equation (5) can be approximated applying different learning techniques (ranging from parameter estimation to machine learning)[4]. Given this approximation of (5), the estimated value for F_i^s can be used to measure F_e^s as follows:

$$F_e^s = F_s^s - F_i^s(q,\dot{q},\ddot{q}). \tag{6}$$

In the next section we will show how F_e^s can be converted to τ_e, the projection of F_e on the joints. Successively, Section III-C and III-D will show two basic strategies for exploiting τ_e in the regulation of interaction forces. Finally, Section IV will present some experimental result.

B. Wrench to Torques Transformation

In this section we describe how to project an external wrench F_e on the joints of the kinematic chain. In our framework, F_e is not measured in its reference frame $\langle e\rangle$ but on the sensor reference frame $\langle s\rangle$. As briefly sketched in Fig. 5, the first step consists in computing F_e^e the equivalent wrench at the point of application. The second step instead transforms this quantity into $F_e^b \in \mathbb{R}^6$, i.e. F_e expressed in the base frame denoted $\langle b\rangle$. Specifically we have:

$$F_e^b = T_e^b \underbrace{H_s^e F_e^s}_{F_e^e}, \tag{7}$$

where:

$$H_s^e = \begin{bmatrix} R_s^e & 0 \\ S(p_s^e)R_s^e & R_s^e \end{bmatrix}, \quad T_e^b = \begin{bmatrix} R_e^b & 0 \\ 0 & R_e^b \end{bmatrix}. \tag{8}$$

From F_e^b it is straightforward to compute the joint level torques τ_e due to the external force F_e. Specifically we have [14]:

$$\tau_e = \left[J_e^b(q)\right]^\top F_e^b \tag{9}$$

where $J_e^b(q) \in \mathbb{R}^{6\times n}$ is the geometric Jacobian of the transformations from $\langle b\rangle$ to $\langle e\rangle$ (see [14] pag. 117 for details).

The composition of (6), (7) and (9) gives the value of τ_e corresponding to the current sensor reading F_s^s. The value of τ_e can then be used for actively controlling the interaction forces: in Section III-C a torque regulator is introduced, while in III-D the impedance controller is briefly presented.

C. Joint torque regulation

This strategy exploits external joint torque measurements τ_e to react to external perturbations and regulate them to a desired value τ_d. A basic control strategy is the following:

$$u = -K_p \cdot T^{-\top} \cdot (\tau_e - \tau_d) \tag{10}$$

[4]The major assumption is the availability of a dataset $\{F_s^s(t_i), q(t_i), \dot{q}(t_i), \ddot{q}(t_i)\}_{i=1}^N$ collected in absence of external perturbations, i.e. $F_e = 0$.

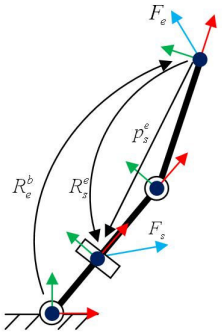

Fig. 5. The F/T sensor transformation scheme. The picture shows the quantities that are necessary for the transformation of equation (7). The sensor $\langle s \rangle$, base $\langle b \rangle$ and end-effector $\langle e \rangle$ frames are sketched. Relative distances and orientations are also shown.

where $u \in \mathbb{R}^n$ is the voltage given to the motors, $K_p \in \mathbb{R}^{n \times n}$ is the gain matrix (typically diagonal) and the matrix $T \in \mathbb{R}^{n \times n}$ accounts for possible differential joints and allows to transform joint torques in motor torques as described in (2). More complex controllers will be proposed in Section IV.

D. Joint impedance control

Exploiting the control strategy (10), an impedance controller can be easily obtained by imposing:

$$\tau_d = -K_d(q - q_d) \tag{11}$$

being $K_d \in \mathbb{R}^{n \times n}$ the diagonal matrix of desired virtual joint stiffness. This controller simulates virtual springs attached to each joint, with stiffness defined by the diagonal elements of K_d and equilibrium points defined by $q_d \in \mathbb{R}^n$.

IV. Experiments

In this section we discuss the implementation of (10) and (11) on the iCub right arm. The proposed method has been easily applied to all the other limbs of the platform, thanks to the modularity of the software and hardware architecture, as described in Section II. The iKin[5] libraries have been used for the robot kinematic definition. It is important to underline that performances will be analyzed within the scope of applications outlined in Section I: specifically, our goal here is not to push the controller performances to their maximum but to show that the achieved results comply with the range of intended applications for the iCub.

In the proposed experiments, the very first step consists in tuning the joint torque regulator (10), studying the transfer function from the motor voltage u to joint projection of the external forces τ_e. In general, this transfer function depends on the external environment and the associated regulation problem might be challenging when no *a priori* knowledge of the environment is available [17]. In our specific case, in order to overcome these issues, we formally neglected internal wrenches (i.e. $F_i = 0$) and treated them as external. This allows us to better tune the joint torque controller taking into account the robot structural resonances (see Section IV-B below). In practice, we study the transfer function from u to τ where:

$$\tau = \left[J_e^b(q)\right]^\top T_e^b H_s^e F_s^s, \tag{12}$$

which is the composition of (6), (7) and (9) assuming $F_i = 0$ (since internal wrenches are considered as external).

A. Open Loop Transfer Function Analysis

We present here the identification of the transfer function from u to τ focusing on a single joint, the iCub elbow. Given the measurement of τ presented in (12), we performed a frequency analysis of the transfer function $P(s)$ between the motor applied voltage u and the measured joint torque τ. The transfer function has been identified with a non parametric identification method. The input u used for creating the identification dataset is a sinusoidal signal with a time varying frequency from $1Hz$ up to $13Hz$. The identified $P(s)$ is plotted in Fig. 6. The system is characterized by a zero at very low frequency and a first resonance peak around $5Hz$; it has been extensively proved [18] that the resonance can be explained by the elasticities in the system which, in our case, are due to the tendon driven actuation and the harmonic drive gear boxes.

B. Torque regulator analysis

Given the frequency characteristics of the transfer function $P(s)$ between u and τ, we considered the possibility of implementing the different regulators proposed in [18] in order to improve the performances of the simple proportional controller described by (10). The final solution is based on a low-pass filter with the following transfer function:

$$C_\omega(s) = k_p \frac{\omega}{s + \omega}, \tag{13}$$

where k_p is the usual proportional gain and where the pole ω should be chosen so as to reduce the effects of the resonance while preserving a sufficient bandwidth[6]. Given the characteristics of the identified transfer function, we tested different values for ω ranging from $1Hz$ to $3Hz$. The effect of $C_\omega(s)$ on $P(s)$ are shown in Fig. 7 representing the different transfer functions $C_\omega(s)P(s)$. It is clear that the effect of the filter is to reduce the amplitude of the resonant peak, by flattening the overall transfer function. In our experiments we eventually chose $\omega = 2Hz$ which give a substantial flattening of the system, while limiting the phase delay of the controller.

C. Impedance Control Analysis

To further demonstrate the effectiveness of the proposed approach, we implemented a joint space impedance controller as described in (11) but exploiting the underlying

[5]iKin is a C++ set of classes for forward-inverse kinematics of serial-links chains of revolute joints with standard Denavit-Hartenberg notation, adopting SI units. It is a part of an open source software project called iCub, released under a GPL license.

[6]Remarkably, given the range of applications outlined in Section I, we do not need to guarantee extremely wide bandwidth.

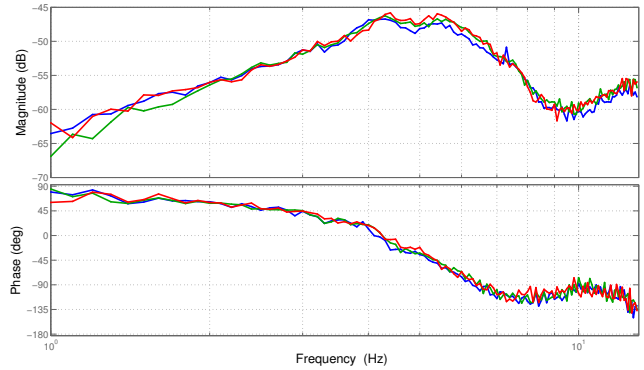

Fig. 6. Bode diagram of the transfer function $P(s)$ between u (input: voltage applied to the elbow motor) and τ (output: measured torque at the elbow joint). Note that τ is an indirect measure since it is obtained using (12). It is noticeable that the system present a zero at low frequency and a resonance at around $5Hz$. The Figure also shows in different colors the transfer function estimated in different trials to prove the repeatability of the identification procedure.

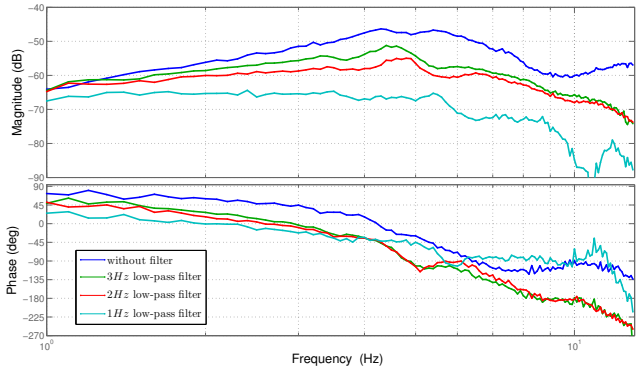

Fig. 7. Bode diagram of the transfer function $C_\omega(s)P(s)$ for different values of ω. The amplitude of the resonance peak decreases with the frequency of the pole of the filter. The more $\omega \to 0$, the flatter the transfer function at a cost of an higher phase delay.

	Measured values for: $k\frac{Nm}{rad}$		
$Joint$	$k_d = 0.6$	$k_d = 0.3$	$k_d = 0.1$
1	0.5839	0.2750	0.1075
2	0.4672	0.3212	0.0897
3	0.5898	0.3506	0.0733
4	0.5269	0.2603	0.0890

TABLE I

PERFORMANCES OF THE STIFFNESS CONTROLLER.

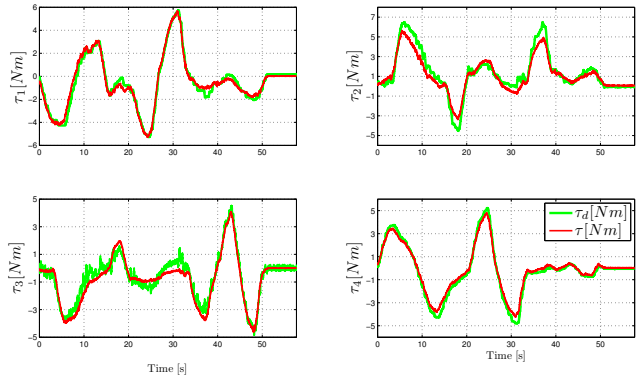

Fig. 8. Torque control: desired (green line) vs. actual (red line) external joint torques. It is here shown the torque regulation resulting from the application of the controller proposed in Section IV-B. The method has been applied to four joints of the iCub right arm. The desired torque τ_d derives from the impedance regulator as described in (11).

force control loop described in Section IV-B[7] on four joints of the iCub right arm. We initially tested $K_d = I \cdot k_d$ with $k_d = 0.6\frac{Nm}{rad}$; corresponding results are shown in Fig. 8 and Fig. 9. In particular, Fig. 8 shows a good agreement between the desired and measured joint torque, which in other terms prove the efficiency of the underlying force control loop. The agreement between desired and actual stiffness is represented in Fig. 9, showing for each joint the desired stiffness (black dashed line), the "position VS force" measured data (green dots), the line fitted to these data (solid red line) and the 95% confidence interval for fitted line (red dashed lines). Finally, Fig. 10 shows the ideal and actual stiffness of each joint in three experimental conditions: $k_d = 0.1\frac{Nm}{rad}$, $k_d = 0.3\frac{Nm}{rad}$ and $k_d = 0.6\frac{Nm}{rad}$. Numerical data for this plot can be found in Table I where k_d is the desired stiffness and k is the stiffness estimated from data.

V. CONCLUSIONS AND FUTURE WORKS

The paper shows a method for achieving force control using localized proximal F/T sensors. The method relies on the transformation of the sensed wrenches from the sensor reference frame to the point of application reference frame. The main assumption is the knowledge of the position where the external perturbation is applied. Force and impedance regulators have been implemented by exploiting the proposed approach. The effectiveness of the controllers has been tested and validated taking into account the targeted applications and goals. The method is sufficiently modular to be easily applied to the four limbs of the humanoid robot iCub. Moreover, the method can be used to implement active compliance in non passively back-drivable manipulators by simply inserting one or more F/T sensors anywhere (but typically where space is available) in the kinematic chain.

Future works will explore different research directions. Primarily, the iCub will be soon sensorized with a distributed tactile sensor system which will be used to determine the contact points where external perturbations are applied, thus removing our current assumption of known contacts locations. Along a different line, we will explore the possibility of fusing the F/T sensor information with other data sources (e.g. joint level torque sensors or other remote F/T sensors).

[7]The impedance controller has been applied to four joints of the iCub right arm, nominally three joint of the shoulder and the elbow. It is worth noting that given the modularity of the proposed approach, the impedance controller has been easily ported to all the four limbs. Reported results are limited to the right arm for sake of clarity.

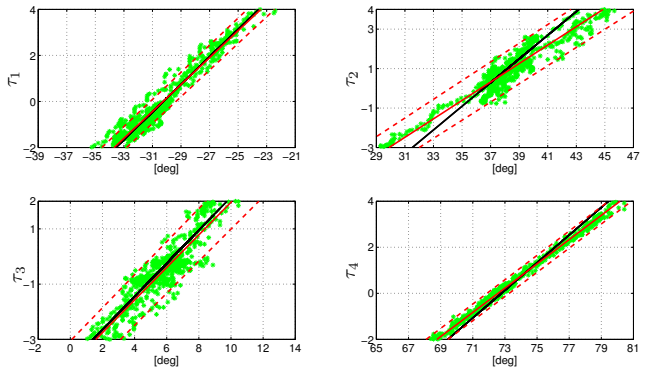

Fig. 9. Impedance control: desired (black solid line) and measured (red solid line) stiffness resulting from the application of the impedance controller (11) to four different joints of the iCub right arm in $q_d = [-30, 37, 6, 73]^\top$. The measured line is the result of linear fitting the measured data points (represented by green dots). A 95% confidence interval for the measured stiffness is represented with red dashed lines.

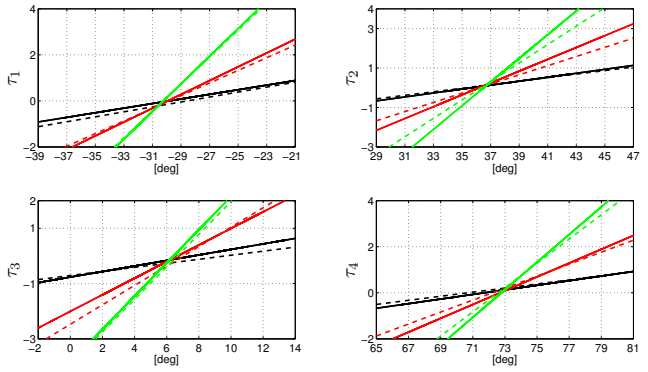

Fig. 10. Impedance control: desired (solid lines) and measured (dashed lines) stiffness resulting from the application of the impedance controller (11) on four joints of the right arm in $q_d = [-30, 37, 6, 73]^\top$. Three different stiffness have been simulated: $k_d = 0.1\frac{Nm}{rad}$ (black lines), $k_d = 0.3\frac{Nm}{rad}$ (red lines), $k_d = 0.6\frac{Nm}{rad}$ (green lines).

VI. ACKNOWLEDGMENTS

The authors were supported by the RobotCub project (IST-2004-004370) and by FP7 project CHRIS (FP7-IST-215805).

REFERENCES

[1] G. Sandini, G. Metta, and D. Vernon, "The iCub cognitive humanoid robot: An open-system research platform for enactive cognition," *50 Years of AI*, vol. LNAI 4850, pp. 359–370, 2007.

[2] A. Desantis, B. Siciliano, A. Deluca, and A. Bicchi, "An atlas of physical humanrobot interaction," *Mechanism and Machine Theory*, vol. 43, no. 3, pp. 253–270, March 2008.

[3] R. Schiavi, B. A., and F. Flacco, "Integration of active and passive compliance control for safe human-robot coexistence," in *2009 IEEE International Conference on Robotics and Automation*, Kobe International Conference Center, Kobe, Japan, 12-17 May 2009.

[4] M. Zinn, O. Khatib, B. Roth, and J. Salisbury, "Playing it safe - human-friendly robots," *Robotics & Automation Magazine, IEEE*, vol. 11, no. 2, pp. 12–21, 2004.

[5] G. Pratt and M. Williamson, "Series elastic actuators," in *Proc. IEEE/RSJ Int. Conf. Intell. Robots Syst.*, vol. 1, Pittsburgh, PA, 1995, pp. 399–406.

[6] R. Schiavi, G. Grioli, S. Sen, and A. Bicchi, "VSA-II: a novel prototype of variable stiffness actuator for safe and performing robots interacting with humans," in *2008 IEEE International Conference on Robotics and Automation*, Pasadena, CA, USA, 19-23 May 2008.

[7] S. Haddadin, A. Albu-Schaffer, and G. Hirzinger, "Safety evaluation of phisical human-robot interaction via crash-testing," in *Robotics: Science and System Conference (RSS 2007)*, Atlanta, Georgia, 2007.

[8] M. Zinn, O. Khatib, B. Roth, and J. Salisbury, "A new actuation approach for human friendly robot design," in *VIII, Springer Tracts in Advanced Robotics*, B. Siciliano and E. P. Dario, Eds., Berlin: Spinger-Verlag, 2002.

[9] B. Siciliano and L. Villani, *Robot Force Control*. Norwell, MA, USA: Kluwer Academic Publishers, 2000.

[10] A. Parmiggiani, M. Randazzo, L. Natale, G. Metta, and G. Sandini, "Joint torque sensing for the upper-body of the iCub humanoid robot," in *International Conference on Humanoid Robots*, Paris, France, 2009.

[11] G. Hirzinger, N. Sporer, A. Albu-Schaffer, M. Hahnle, R. Krenn, A. Pascuccum, and M. Schedl, "DLR's torque-controlled light weight robot III - are we reaching the technological limits now?" *Robotics and Automation, 2002. Proceedings ICRA '02 IEEE International Conference on*, vol. 2, pp. 1710–1716, 2002.

[12] N. Tsagarakis, G. Metta, G. Sandini, D. Vernon, R. Beira, J. Santos-Victor, M. Carrazzo, F. Becchi, and D. Caldwell, "icub - the design and realization of an open humanoid platform for cognitive and neuroscience research," *International Journal of Advanced Robotics*, vol. 21(10), pp. 1151–75, Oct. 2007.

[13] G. Metta, G. Sandini, D. Vernon, L. Natale, and F. Nori, "The iCub humanoid robot: an open platform for research in embodied cognition," in *PerMIS: Performance Metrics for Intelligent Systems Workshop*, Washington DC, USA, Aug 19-21, 2008.

[14] L. Sciavicco and B. Siciliano, *Modelling and Control of Robot Manipulators*, 2nd ed., ser. Advanced Textbooks in Control and Signal Processing series. London: Springer, 2005.

[15] N. Tsagarakis, F. Becchi, L. Righetti, A. Ijspeert, and D. Caldwell, "Lower body realization of the baby humanoid - iCub," in *IEEE/RSJ International Conference on Intelligent Robots and Systems*, San Diego, USA, Oct-Nov 2007.

[16] M. Fumagalli, A. Gijsberts, S. Ivaldi, L. Jamone, G. Metta, L. Natale, F. Nori, and G. Sandini, *Learning to Exploit Proximal Force Sensing: a Comparison Approach*, ser. Studies in Computational Intelligence. Springer-Verlag Berlin and Heidelberg GmbH & Co. K, 2010, vol. Volume 264/2010, pp. 149–167.

[17] E. Colgate and N. Hogan, *The Interaction of Robots with Passive Environments: Application to Force Feedback Control.*, ser. Advanced Robotics 1989, e. Kenneth J. Waldron, Ed. Berlin: Springer-Verlag, 1989.

[18] R. Volpe and P. Khosla, "A theoretical and experimental investigation of explicit force control strategies for manipulators," *IEEE Transactions on Automatic Control*, vol. 38(11), pp. 1634–1650, November 1993.